Microfluid Nanofluid (2012) 13:125–130
DOI 10.1007/s10404-012-0949-z

RESEARCH PAPER

Explaining high flow rate of water in carbon nanotubes via solid–liquid molecular interactions

Davide Mattia · Francesco Calabrò

Received: 26 October 2011 / Accepted: 1 February 2012 / Published online: 21 February 2012

Abstract Experimental and simulation measurements of water flow through carbon nanotubes have shown orders of magnitude higher flow rates than what was predicted using continuum fluid mechanics models. Different explanations have been offered, from slippage of water on the hydrophobic surface of the nanotubes to size confinement effects. In this work a model capable of explaining these observations, linking the enhanced flow rates observed to the solid–liquid molecular interactions at the nanotube wall is proposed. The model is capable of separating the effects on flow enhancement of the tube characteristic dimensions and the solid–liquid molecular interactions, accurately predicting the effect of each component for nanotubes of different sizes, wall surface chemistry and structure. Comparison with the experimental data available shows good agreement.

Keywords Carbon nanotubes · Nanofluidics · Work of adhesion · Slip

1 Introduction

Experimental results have shown higher than expected water flow rates through carbon nanotubes (CNTs) with enhancements of up to 10,000 times compared to the values calculated using classical continuum fluid mechanics models used at the macroscale (Whitby and Quirke 2007; Mattia and Gogotsi 2008). The available results cover a wide range of CNT diameters (0.8–44 nm) and lengths (2–280 μm), wall structures (from fully ordered and graphitic to disordered turbostratic carbon) and applied pressures (0.1–100 MPa), (Holt et al. 2006; Majumder et al. 2005, 2011; Whitby et al. 2008; Qin et al. 2011). Molecular dynamics (MD) simulations of water flow through CNTs have shown comparably high enhancements, while suggesting that this effect is due to the specific interactions between the nanotube wall and the fluid (Joseph and Aluru 2008; Thomas and McGaughey 2008; Thomas et al. 2010; Nicholls et al. 2011). This has been in part confirmed by experiments showing that the wettability of CNTs by water can be controlled by modifying the nanotubes' wall surface chemistry and structure (Mattia et al. 2006a, b; Majumder and Corry 2011).

Despite these results, an explicit dependence of the water flow rate through CNTs on the tubes' radius, wall surface chemistry or structure has not yet been determined. This is mainly due to the absence of an explicit term linking solid–liquid molecular interactions to flow in the Navier–Stokes equations. In classical fluid dynamics this limitation is overcome using semi-empirical parameters such as the friction factor (Celata et al. 2006), which are not necessarily applicable at the nanoscale and, in any case, do not explain the origin of the observed effects. In the experimental conditions used in the papers cited above, the Navier–Stokes equations reduce to the Haagen–Poiseuille equation with slip at the wall. As such, a majority of researchers have, so far, focused on establishing an indirect link via the slip length, a parameter defined as the hypothetical distance from the channel wall where the extrapolation of the parabolic velocity profile reaches zero (Neto

D. Mattia (✉)
Department of Chemical Engineering,
University of Bath, Bath BA27AY, UK
e-mail: d.mattia@bath.ac.uk

F. Calabrò
DAEIMI Department, University of Cassino,
03043 Cassino, Italy

et al. 2005). The slip length has been related to measurable quantities such as contact angle, roughness, viscosity and others (Lauga et al. 2005). The dependence of the slip length with the contact angle is the most interesting, since it is intuitive to think that how a liquid wets a surface can affect how it flows onto it, even though no contact angle is present in the conditions where the Haagen–Poiseuille equation is used as there is no liquid–vapour interface. The best known model relating the contact angle to the slip length, originally developed by Tolstoi, is based on the difference in mobility between fluid molecules in contact with a hydrophobic wall and those in the bulk (Blake 1990). This model assumes that when a polar liquid, such as water, is in contact with a hydrophobic surface, the attraction between liquid molecules is stronger than the attraction of the same molecules to the solid (Israelachvili 1991; Zettlemoyer 1968), as confirmed by contact angle and surface force apparatus measurements (Fox and Zisman 1950; Neto et al. 2005). As a consequence, liquid molecules will try to minimize the interaction with the surface, leading to an increased velocity compared to bulk molecules, under the action of an external field such as a pressure gradient. On a hydrophilic surface, on the other hand, polar liquid molecules would be slowed down due to a more favourable solid–liquid interaction. While this model envisages an exponential dependence of the slip length on the contact angle, which could potentially justify the high enhancement values observed experimentally, it is based on hard to measure parameters referring to the solid–liquid couple. A partial solution to this problem has been proposed in (Myers 2010), where the liquid flowing through a CNT is modelled as a two-phase system with the water molecules in a thin annular region near the tube wall having different transport properties than the bulk liquid. This model is in agreement with MD simulations showing different liquid concentrations at the wall compared to the bulk (Joseph and Aluru 2008). Furthermore, one can focus on the non-zero velocity at the wall which, unlike the slip length, has a clear physical meaning. Based on the same premises as Tolstoi's theory, Ruckenstein derived a model for the velocity at the wall as a function of the surface diffusion of water molecules on a hydrophobic surface (Ruckenstein and Rajora 1983). The diffusion along the tube surface is due to the chemical potential gradient caused by the pressure gradient along the tube.

In this paper, a model capable of separating the effects on flow enhancement of the tube characteristic dimensions and the solid–liquid molecular interactions, accurately predicting the effect of each component for nanotubes of different sizes, wall surface chemistry and structure has been derived. This has been achieved by deriving a novel expression for the velocity at the wall. Comparison with experimental and MD data shows good agreement.

2 Fluid flow model

The proposed model is based on the Haagen–Poiseuille equation for steady state, laminar flow through a pipe with a circular cross section. This model, therefore, lies within the continuum fluid dynamic range. MD results have shown that this is the case for nanotubes with diameters equal to or greater than 1.66 nm (Thomas and McGaughey 2009). A two-fluid system with reduced viscosity in an annular region close to the wall (Myers 2010) has been adopted to account for variations in liquid density observed in MD simulations (Thomas and McGaughey 2008; Pascal et al. 2011) and predicted by Tolstoi's model:

$$\begin{aligned} u_1(r) &= -\frac{\Delta p}{L}\frac{1}{4\mu_1}r^2 + c_1,\ r \in [0, R-\delta] \\ u_2(r) &= -\frac{\Delta p}{L}\frac{1}{4\mu_2}r^2 + c_2,\ r \in [R-\delta, R] \end{aligned} \tag{1}$$

where $u_i (i = 1, 2)$ and $\mu_i (i = 1, 2)$ are the velocity in the axial direction of the tube and the dynamic viscosity, respectively, in the two regions of the pipe, and $\Delta p/L$ is the externally applied pressure gradient; the other terms in the equation are defined in Fig. 1. Here μ_1 is assumed to be equal to the bulk water viscosity (Thomas and McGaughey 2008).

The boundary conditions that guarantee continuity of the velocity and of the shear stress and mass conservation are:

$$\begin{aligned} &\frac{\partial u_1}{\partial r}(r=0) = 0 \\ &u_1(r = R-\delta) = u_2(r = R-\delta) \\ &\mu_1\frac{\partial u_1}{\partial r}(r = R-\delta) = \mu_2\frac{\partial u_2}{\partial r}(r = R-\delta) \\ &-\lambda\frac{\partial u_2}{\partial r}(r = R) = u_2(r = R) \end{aligned} \tag{2}$$

where λ is the slip length.

By solving Eq. 1 with the boundary conditions given in Eq. 2, the velocity profiles are parabolic, and integrating them over the radius of the channel in each section yields the fluid flow, Q. This is the quantity actually measured in the experimental observation discussed in the Sect. 1. The flow enhancement is defined as the ratio of experimental

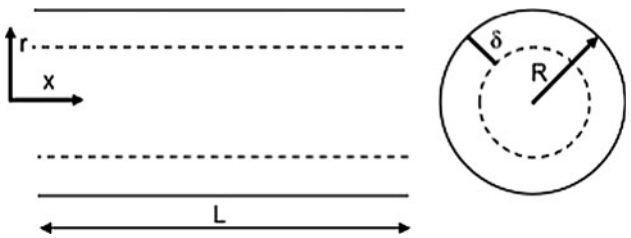

Fig. 1 Schematic of the geometry of the two-fluid model for water flow inside carbon nanotubes

(or novel model) Q over the no-slip Haagen–Poiseuille one, where $\lambda = \delta = 0$:

$$\varepsilon_{\lambda,\delta} = \frac{Q_{\lambda,\delta}}{Q_{\lambda=\delta=0}} = \left(\frac{R-\delta}{R}\right)^4 \left(1 - \frac{\mu_1}{\mu_2}\right) + \frac{\mu_1}{\mu_2}\left(1 + \frac{4\lambda}{R}\right) \tag{3}$$

This is a more general expression for the flow enhancement and it depends on the choice of the three parameters μ_2, δ and λ. The first two can be fixed following previous reports: The thickness of the annular region at the wall is taken as $\delta = 0.7$ nm, approximately two water molecule diameters (Myers 2010; Joseph and Aluru 2008). Values for μ_2 have been found to be a function of the tube diameter (Thomas and McGaughey 2008), as reported in Appendix A.

3 Effect of solid–liquid interactions on flow velocity

Once μ_2 and δ are fixed, the sole remaining parameter in the equations above is λ. As discussed in the Sect. 1, the physical meaning of this parameter is not clear. From Eq. 2, an expression for λ as a function of the velocity at the wall, $u(r = R)$, can be derived:

$$\lambda = \frac{L}{\Delta p}\frac{2\mu_2}{R}u(r = R) \tag{4}$$

When $u_R = 0 \Rightarrow \lambda = 0$ and the no-slip boundary condition is recovered. This is the case in (Myers 2010), where any enhancement effect is due solely to the μ_2/μ_1 ratio. However, this is not sufficient to explain the high enhancements observed experimentally (Mattia and Gogotsi 2008). In addition, Tolstoi's model assumes that the presence of a reduced viscosity region near the wall implies a non-zero velocity at the wall (Blake 1990). Ruckenstein, following Tolstoi's model, derived an expression for the velocity at the wall that is linearly proportional to the applied pressure gradient and the diffusion of fluid molecules along the surface of the tube (Ruckenstein and Rajora 1983):

$$u(r = R) = \frac{D_s}{k_B T n_L}\frac{\Delta p}{L} \tag{5}$$

where $n_L$is the number of molecules per unit volume in the interfacial region, D_s is the surface diffusion and k_B and T are Boltzmann's constant and temperature, respectively. Recent MD simulations of surface diffusion of water in hydrophobic and hydrophilic slits and channels have shown that the lower the interaction energy between the liquid and the solid, the higher the surface diffusion. For example, values for $D_s \sim (2-4)\cdot 10^{-9}$ m^2 s^{-1} have been obtained for graphene-water and CNT-water and $D_s \sim 1\cdot 10^{-9}$ m^2 s^{-1} for hydrophilic titania-water systems (Park and Aluru 2010; Martí et al. 2010). Eq. 5, therefore, predicts higher values of the velocity at the wall for water flowing through hydrophobic channels, as discussed earlier.

In the present work, it is observed that the term $k_B T n_L L$ in Eq. 5 is the energy per unit surface of the monolayer of fluid molecules at the interface with the solid. This energy is given by the molecular interactions between the liquid molecules and the tube's wall per unit surface (Israelachvili 1991). In other words, it represents the solid–liquid interaction energy per unit surface, or work of adhesion, W_A (Harkins 1952). As a consequence, it is proposed here that the velocity at the wall is expressed as:

$$u(r = R) \equiv u_R = \frac{D_s}{W_A}\Delta p \tag{6}$$

Using u_R in Eq. 1 yields a parabolic velocity profile, with a non-zero velocity at the wall (see Appendix A).

The work of adhesion is defined as the work necessary to separate a liquid from a solid to create two new interfaces (Harkins 1952; Zisman 1964):

$$W_A = \pi_e + \gamma_{LV}(1 + cos\theta) \tag{7}$$

where π_e is the film pressure of the adsorbed vapour, γ_{LV} is the liquid–vapour surface tension and θ is the contact angle, as defined by Young's equation. Values for the work of adhesion can also be independently evaluated via heat of immersion experiments (Harkins 1952).

The higher the value of W_A, the stronger the adhesion between the solid and the liquid. In fact, for water on graphite $\pi_e = 19$ mJ m^{-2} and $\theta = 86°$, giving $W_A \sim 97$ mJ m^{-2} (Mattia and Gogotsi 2008), whereas the value for a high energy, hydrophilic surface like titania is ~ 350 mJ m^{-2}, and for a more hydrophobic material like PTFE the value reduces to ~ 36 mJ m^{-2} (Harkins 1952). The work of adhesion term is also capable of accounting for variations in the surface chemistry and structure of the solid wall due to its dependency on the contact angle. It is well established that graphitic CNTs have a contact angle of 80°–86° (Mattia and Gogotsi 2008), and that the presence of defects on the walls of CNTs can significantly alter their wettability (Werder et al. 2003). In the case of the largest CNTs used so far for flow experiments, for example, the synthesis method produces a turbostratic graphitic structure, with a high density of surface defects and functional groups (Whitby et al. 2008). This results in a reduction of the water contact angle in these CNTs (Mattia et al. 2006b), with a consequent increase of the work of adhesion. For water on the nanotubes used in (Whitby et al. 2008), contact angles vary between $\sim 80°$ and $\sim 40°$ depending on the synthesis and post-processing treatment (Mattia et al. 2006b). Assuming $\pi_e = 19$ mJ m^{-2} in this case as well, the former contact angle value yields

$W_A \approx 105$ mJ m^{-2}, while the latter gives $W_A \approx 144$ mJ m^{-2}.

The key conclusion of Eq. 6 is that the velocity at the wall is solely a function of the solid–liquid molecular interactions at the wall and is not a function of the tube characteristics or the pressure gradient. The overall velocity profile, on the other hand, remains a function of both (Appendix A). The proposed formulation is in agreement with MD observations that the high flow rates observed for carbon nanotubes are associated with low interaction energies between water and the sp^2 carbon structure of CNTs (Thomas and McGaughey 2008, 2009; Thomas et al. 2010; Werder et al. 2003; Walther et al. 2004; Majumder and Corry 2011). In fact, a low interaction energy results in a low value of W_A and a high value of D_s, yielding a high velocity at the wall, in agreement with Tolstoi's model.

4 Comparison with experimental data

As discussed in the Sect. 1, the flow enhancement has been used as a measure of the difference in flow behavior in nanotubes compared to macroscopic flow. Here, it will be used to show how the proposed model fares against experimental and MD data. Once a solid–liquid couple has been fixed, replacing Eq. 6 in Eq. 3 yields an expression for the flow enhancement incorporating the proposed dependence on the solid–liquid interactions:

$$\varepsilon = \left(\frac{R-\delta}{R}\right)^4 \left(1-\frac{\mu_1}{\mu_2}\right) + \frac{\mu_1}{\mu_2}\left(1 + 8\mu_2 \frac{L}{R^2}\frac{D_s}{W_A}\right) \qquad (8)$$

Using experimental data for pressure, channel dimensions and other relevant parameters, enhancement values from Eq. 8 have been compared to experimental and MD literature results (Table 1). Specific values of all the parameters used can be found in Appendix B. Comparison to experimental and MD data has been limited to cases where the nanotube diameter is above 2 nm (the threshold for the validity of the continuum fluid mechanics model) and values of the parameter required in Eqs. 6 and 8 are available.

As it can be seen in Table 1, the enhancement values calculated according to Eq. 8 are compatible with published data except for the paper from Majumder et al. (2005), which shows flow enhancements significantly higher than other reported values. MD simulations (Thomas et al. 2010; Thomas and McGaughey 2008) for the same geometrical and pressure values of (Majumder et al. 2005) have similarly shown significantly smaller enhancements.

Calculations using data in Table 1 and Appendix Table 2 show that the first term of Eq. 8 is always negligible compared to the second one, and that $8\mu_2 \frac{L}{R^2}\frac{D_s}{W_A} \gg 1$. Therefore Eq. 8 can be simplified as:

$$\varepsilon \approx 8\mu_1 \frac{L}{R^2}\frac{D_s}{W_A} \qquad (9)$$

This expression makes explicit the contribution to the flow enhancement of the tube characteristic dimensions and of the solid–liquid interaction parameters.

When Eq. 9 is used to separate the contribution of the solid–liquid interactions to the enhancement from those of the tube geometrical characteristics, a dependence of the enhancement on $1/R^2$ is observed (Fig. 2). This applies to all types of nanotubes, normalized for different lengths. This formulation explains why smaller nanotubes have shown higher enhancements without resorting to slip length values that are orders of magnitude larger than the tubes' diameter (Neto et al. 2005) or additional fitting parameters (Thomas et al. 2010; Myers 2010). The very close agreement with MD data (open symbols in Fig. 2) is due to the fact that the solid–molecular interactions effects on flow are implicit in the carbon–water potentials used in MD, whereas they are made explicit in Eq. 6.

Finally, it is noted here that the complete expression of ε in Eq. 8 implies that the flow enhancement value will always be larger than one, for any tube radius. A similar conclusion has been suggested by MD predictions of $\varepsilon \approx 2$

Table 1 Comparison of calculated flow enhancement values using to experimental and MD results available in literature

Reference	CNT		Flow enhancement, ε	
	R (nm)	L (μm)	Literature	Eq. 10
Thomas and McGaughey (2009)	0.88	75×10^{-3}	20 ± 2	10–20
Holt et al. (2006)	1.0	2–3	560–8,400	290–880
Thomas et al. (2010)	1.38	1	110 ± 5	80–150
Majumder et al. (2005)	3.5	34–126	$(43–77) \times 10^3$	400–3,000
Du et al. (2011)	5	4,000	$(88–360) \times 10^3$	$(23–46) \times 10^3$
Whitby et al. (2008)	23 ± 1	78 ± 2	20–37	7–24

The range of calculated enhancements is due to variations of geometrical and interaction parameters used (Appendix B)

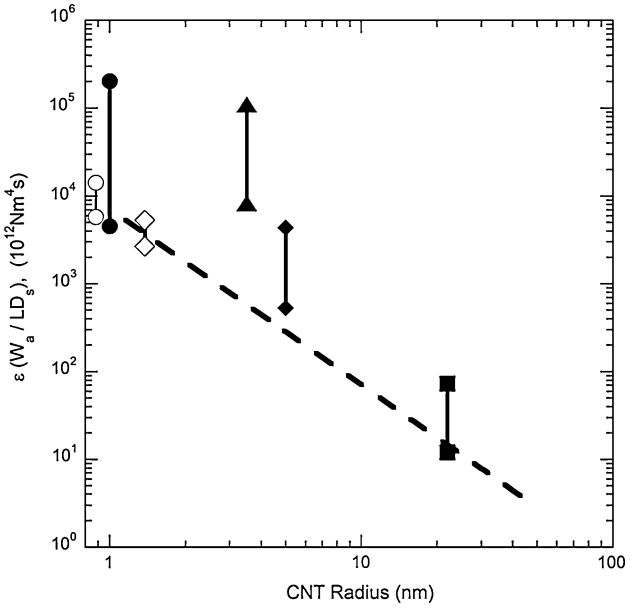

Fig. 2 Normalized flow enhancement as a function of carbon nanotube radius (*dashed curve*). The literature enhancement ranges reported in Table 1 have been normalized for comparison: *Circle* Thomas and McGaughey (2009); *filled circle* Holt et al. (2006); *diamond* Thomas et al. (2010); *filled triangle* Majumder et al. (2005); *filled diamond* Du et al. (2011); *filled square* Whitby and Quirke (2007). The literature values (*open symbols* for MD and *full symbols* for experimental) are reported as a range between minimum and maximum possible values

for 250 nm diameter CNTs (Thomas and McGaughey 2008). No measurable enhancement was observed for water flow measurements in carbon nanopipes with diameter of 300–500 nm (Sinha et al. 2007). In this case, Eq. 8 predicts a flow enhancement between 0.1 and 1%, below the experimental error. This shows why the no-slip boundary condition well reproduces velocity profiles in both micro and macroscale tubes.

5 Conclusions

This paper attempts to make explicit in the Haagen–Poiseuille equation the effect on flow of the solid–liquid molecular interactions, via macroscopic quantities, the work of adhesion and surface diffusion. These can be measured independently once a solid–liquid couple has been chosen. The results show that the proposed model can separate the effects on flow enhancement of the tube characteristic dimensions and the solid–liquid molecular interactions, accurately predicting the effect of each component for CNTs of different sizes, wall surface chemistry and structure. The present model is not limited to carbon nanotubes as water, but it will be possible to extend it to other systems provided that values for the work of adhesion and surface diffusion can be measured or calculated independently.

Acknowledgments Work on this project was supported by a UK Royal Society International Joint Research Grant. DM is also supported by a UK Royal Academy of Engineering Research Fellowship.

Appendix A: velocity profile equations

The velocity profiles derived from Eq. 1 using the boundary conditions in Eq. 2 yield:

$$u_1(r) = \frac{\Delta p}{L}\frac{1}{4\mu_2}\left(R^2 - \frac{\mu_2}{\mu_1}r^2\right) + \frac{\lambda R}{2L\mu_2}\Delta p + \frac{\Delta p}{L}\frac{\mu_2-\mu_1}{4\mu_1\mu_2}(R-\delta)^2,\ r \in [0, R-\delta] \quad (10)$$

$$u_2(r) = \frac{\Delta p}{L}\frac{1}{4\mu_2}\left(R^2 - r^2\right) + \frac{\lambda R}{2L\mu_2}\Delta p,\ r \in [R-\delta, R]$$

Using Eq. 6 in Eq. 10 yields a parabolic velocity profile, with a non-zero velocity at the wall:

$$u_1(r) = \frac{\Delta p}{L}\frac{1}{4\mu_2}\left(R^2 - \frac{\mu_2}{\mu_1}r^2\right) + \frac{D_s}{W_A}\Delta p + \frac{\Delta p}{L}\frac{\mu_2-\mu_1}{4\mu_1\mu_2}(R-\delta)^2,\ r \in [0, R-\delta] \quad (11)$$

$$u_2(r) = \frac{\Delta p}{L}\frac{1}{4\mu_2}\left(R^2 - r^2\right) + \frac{D_s}{W_A}\Delta p,\ r \in [R-\delta, R]$$

In the bulk region, the three terms on the right-hand side of the equation represent the no-slip solution, the non-zero velocity at the wall and the continuity term, respectively. In the interfacial region, only the first two terms are present. As in the no-slip case, the shape of the parabolic velocity profile is a function of the pressure gradient, whereas the velocity at the wall is only a function of the solid–liquid molecular interactions.

Appendix B: numerical values of parameters used for calculations in Table 1 and Fig. 2

The values of all the parameters used to calculate flow enhancements in Table 1 and Fig. 2 are reported below (Appendix Table 2). It is noted here that in the case of the largest CNTs considered, a higher value of the work of adhesion and a lower value of the diffusion coefficient have been used due to the different nature of the nanotube wall structure and chemistry, as described in Sect. 3. Variable viscosity values as a function of nanotube diameters have been used (Thomas and McGaughey 2008). The different values of the work of adhesion used are discussed in Sect. 3.

Table 2 Parameter values used to calculate enhancement values in Fig. 2 and Table 1

References	D_s (10^{-9} m^2 s^{-1})	W_A (10^{-3} J m^{-2})	μ_2 (10^{-4} Pa s)	δ (nm)	Δp (Pa)
Thomas and McGaughey (2009)	1–2[a]	97	0.6 × μ_1	0.7	75 × 10^5
Holt et al. (2006)	2–4[a]		0.7 × μ_1		10^5
Thomas et al. (2010)					1.38 × 10^8
Majumder et al. (2005)			$\mu_1 = 8.9$		0.8 × 10^5
Du et al. (2011)					10^5
Whitby et al. (2008)	1–2[a]	100–150			10^5

[a] Values from Park and Aluru (2010)

References

Blake TD (1990) Slip between a liquid and a solid: D.M. Tolstoi's (1952) theory reconsidered. Colloids Surf 47:135–145

Celata GP, Cumo M, McPhail S, Zummo G (2006) Characterization of fluid dynamic behaviour and channel wall effects in microtube. Int J Heat Fluid Fl 27(1):135–143. doi:10.1016/j.ijheatfluidflow.2005.03.012

Du F, Qu L, Xia Z, Feng L, Dai L (2011) Membranes of vertically aligned superlong carbon nanotubes. Langmuir 27(13):8437–8443. doi:10.1021/la200995r

Fox HW, Zisman WA (1950) The spreading of liquids on low energy surfaces. Polytetrafluoroethylene. J Colloid Sci 5(6):514

Harkins WD (1952) Physical chemistry of surface films. Reinhold, New York

Holt JK, Park HG, Wang Y, Stadermann M, Artyukhin AB, Grigoropoulos CP, Noy A, Bakajin O (2006) Fast mass transport through sub-2-nanometer carbon nanotubes. Science 312(5776):1034–1037. doi:10.1126/science.1126298

Israelachvili J (1991) Intermolecular and surface forces, 2nd edn. Academic Press, San Diego

Joseph S, Aluru NR (2008) Why are carbon nanotubes fast transporters of water? Nano Lett 8(2):452–458. doi:10.1021/nl072385qS1530-6984(07)02385-5

Lauga E, Brenner MP, Stone HA (2005) Microfluidics: the no-slip boundary condition. In: Foss J, Tropea C, Yarin A (eds) Handbook of experimental fluid dynamics. Springer, New York

Majumder M, Corry B (2011) Anomalous decline of water transport in covalently modified carbon nanotube membranes. Chem Commun 47(27):7683–7685

Majumder M, Chopra N, Andrews R, Hinds BJ (2005) Nanoscale hydrodynamics: enhanced flow in carbon nanotubes. Nature 438(7064):44

Majumder M, Chopra N, Hinds BJ (2011) Mass transport through carbon nanotube membranes in three different regimes: ionic diffusion and gas and liquid flow. ACS Nano 5(5):3867–3877. doi:10.1021/nn200222g

Martí J, Sala J, Guàrdia E (2010) Molecular dynamics simulations of water confined in graphene nanochannels: from ambient to supercritical environments. J Mol Liq 153(1):72–78. doi:10.1016/j.molliq.2009.09.015

Mattia D, Gogotsi Y (2008) Review: static and dynamic behavior of liquids inside carbon nanotubes. Microfluid Nanofluid 5(3):289–305. doi:10.1007/s10404-008-0293-5

Mattia D, Bau HH, Gogotsi Y (2006a) Wetting of CVD carbon films by polar and non-polar liquids and implications for carbon nanopipes. Langmuir 22(4):1789–1794

Mattia D, Rossi MP, Kim BM, Korneva G, Bau HH, Gogotsi Y (2006b) Effect of graphitization on the wettability and electrical conductivity of CVD carbon nanotubes and films. J Phys Chem B 110(20):9850–9855

Myers T (2010) Why are slip lengths so large in carbon nanotubes? Microfluid Nanofluid 10(5):1141–1145. doi:10.1007/s10404-010-0752-7

Neto C, Evans DR, Bonaccurso E, Butt H-J, Craig VSJ (2005) Boundary slip in Newtonian liquids: a review of experimental studies. Rep Prog Phys 68:2859–2897. doi:http://dx.doi.org/10.1088/0034-4885/68/12/R05

Nicholls W, Borg M, Lockerby D, Reese J (2011) Water transport through (7,7) carbon nanotubes of different lengths using molecular dynamics. Microfluid Nanofluid 12(1–4):257–264. doi:10.1007/s10404-011-0869-3

Park JH, Aluru NR (2010) Ordering-induced fast diffusion of nanoscale water film on graphene. J Phys Chem C 114(6):2595–2599. doi:10.1021/jp907512z

Pascal TA, Goddard WA, Jung Y (2011) Entropy and the driving force for the filling of carbon nanotubes with water. Proc Natl Acad Sci 108(29):11794–11798. doi:10.1073/pnas.1108073108

Qin X, Yuan Q, Zhao Y, Xie S, Liu Z (2011) Measurement of the rate of water translocation through carbon nanotubes. Nano Lett: null–null. doi:10.1021/nl200843g

Ruckenstein E, Rajora P (1983) On the no-slip boundary condition of hydrodynamics. J Colloid Interface Sci 96(2):488–491. doi:10.1016/0021-9797(83)90050-4

Sinha S, Rossi MP, Mattia D, Gogotsi Y, Bau HH (2007) Induction and measurement of minute flow rates through nanopipes. Phys Fluids 19(1):013603–013608

Thomas JA, McGaughey AJH (2008) Reassessing fast water transport through carbon nanotubes. Nano Lett 8(9):2788–2793

Thomas JA, McGaughey AJH (2009) Water flow in carbon nanotubes: transition to subcontinuum transport. Phys Rev Lett 102(18):184502

Thomas JA, McGaughey AJH, Kuter-Arnebeck O (2010) Pressure-driven water flow through carbon nanotubes: Insights from molecular dynamics simulation. Int J Therm Sci 49(2):281–289

Walther JH, Werder T, Jaffe RL, Koumoutsakos P (2004) Hydrodynamic properties of carbon nanotubes. Phys Rev E 69(6):062201–062204

Werder T, Walther JH, Jaffe RL, Halicioglu T, Koumoutsakos P (2003) On the water-carbon interaction for use in molecular dynamics simulations of graphite and carbon nanotubes. J Phys Chem B 107(6):1345–1352

Whitby M, Quirke N (2007) Fluid flow in carbon nanotubes and nanopipes. Nat Nano 2:87–94

Whitby M, Cagnon L, Thanou M, Quirke N (2008) Enhanced fluid flow through nanoscale carbon pipes. Nano Lett 8(9):2632–2637. doi:10.1021/nl080705f

Zettlemoyer AC (1968) Hydrophobic surfaces. J Colloid Interface Sci 28(3/4):343365

Zisman WA (1964) Relation of equilibrium contact angle to liquid and solid constitution. In: Fowkes FM (ed) Contact Angle, Wettability, and Adhesion, vol 43. Advances in Chemistry Series. American Chemical Society, Washington D.C., pp 1–56